Volume 1 | Number 1 | Jan 2013 | Pages 1–100

Nanoscale

www.rsc.org/nanoscale

ROYAL SOCIETY OF CHEMISTRY

ROYAL SOCIETY OF CHEMISTRY

www.rsc.org/nanoscale

Journal Name

ARTICLE

One-step fabrication of multifunctional micromotors†

Wenlong Gao,[a] Mei Liu,[a] Limei Liu,[a] Hui Zhang,[a] Bin Dong,*[a] and Christopher Y. Li*[b]

Although artificial micromotor has experienced tremendous progresses in recent years, their fabrication normally requires complex steps or expensive equipment. In this paper, we report a facile one-step method based on an emulsion solvent evaporation process to fabricate multifunctional micromotors. By simultaneously incorporating various components into an oil-in-water droplet, upon emulsification and solidification, a sphere-shaped, asymmetric, and multifunctional micromotor is formed. Some of the attractive functions of this model micromotor include autonomous movement in high ionic strength solution, remote control, enzymatic disassembly and sustained release. This one–step, versatile fabrication method can be easily scaled up and therefore may have great potential in mass producing multifunctional micromotors for a wide range of practical applications.

Introduction

Since the concept of catalytic motor was proposed by Whitesides et al.,[1] the researches on this topic have undergone tremendous progresses during the past decade.[2-7] Currently, efforts in this field have been exerted on the development of artificial motors at microscale.[8-10] Recent progresses have demonstrated that tiny micromotors, which can move autonomously in the fluidic environment, have great potential in a variety of different applications ranging from cargo transportation, cell separation, targeted delivery, to environmental remediation.[7,11-13] To fabricate such devices, it is advantageous to use asymmetric micromotors, either in shape or in composition. The asymmetry provides the differences in the properties, such as catalytic activities, from the different compartments within a single micromotor. As a result, it leads to the generation of unidirectional propulsion forces upon the addition of a suitable fuel, which is essential for a micromotor to achieve motion in the fluidic environment.

For a micromotor, in order to build the asymmetric structure, various materials with different functions are generally introduced and combined together in certain geometry. For example, thin layers of a variety of catalytically active metals, including platinum,[14] iridium,[15] etc. can be directly deposited onto the surface of a microsphere made of silicon dioxide,[16] magnesium,[17] etc. The resulting structure possesses an asymmetric feature, i.e. active materials decorate only part of the surfaces of the inert ones, which is a desired configuration for the micromotor. Template synthesis is another widely used method to construct micromotors.[18-20] Based on the microporous filter membrane template (made of polycarbonate or aluminum oxide) and the electrochemical deposition method, by simply changing the composition of the plating solution, different

materials including metals (platinum, nickel, gold) or conducting polymers can be easily introduced into the pores in a layer-by-layer fashion.[2,3,10] As a consequence, two different types of asymmetric structures can be generated: microrods comprising multiple segments and microtubes made of various functional material layers.[2,3,18] By utilizing microfabrication methods such as photolithography or shadow mask evaporation, micromotors based on roll-up tubes consisting of different metal layers have also been developed.[6,21] Despite these progresses, currently established methods contain multiple steps and sometimes require the utilization of expensive equipments, which greatly hinder the further development of micromotor in different practical applications. Therefore, developing micromotor synthesized by a single-step and low cost method is urgently needed.

In this paper, we report a one-step fabrication method to obtain multifunctional micromotors. This method is based on an emulsion solvent evaporation technique. Unlike the previously developed methods to construct a micromotor in a stepwise fashion, all components of the current micromotor, such as biodegradable polycaprolactone (PCL), catalytically active platinum nanoparticles (PtNPs) and other functional materials including magnetic iron oxide nanoparticles (Fe_3O_4NPs) and fluorescent coumarin molecules are introduced simultaneously within a single step. The resulting micromotor possesses an asymmetric structure. Not only can this micromotor move autonomously in salt solution upon the addition of a fuel, it also exhibits multiple functions, such as magnetic control, enzymatic disassembly and sustained release. The simple, scalable fabrication process and the multiple functionalities of the resultant micromotor make our approach an attractive candidate to produce micromotors for practical applications.

Experimental

Materials

PtNP (100-500 nm), coumarin and Fe_3O_4NP (20 nm) were purchased from Aladdin reagent. PCL was synthesized according to the literature method.[22] Sodium dodecyl sulfate (SDS) was obtained from Sinochemical Inc. Lipase from Pseudomonas cepacia and PBS solution were purchased from Sigma-Aldrich Company. Magnetic nanoparticle-coated polystyrene beads were purchased from Spherotech Inc.

Preparation of the micromotors

A typical fabrication method is as follows: 1 mL chloroform phase containing 4 mg PtNP, 4 mg Fe_3O_4NP, 20 mg coumarin and 100 mg PCL was dissolved/dispersed in a continuous water phase (30 mL) containing 1 w/v% SDS by vigorous agitation. After solvent evaporation for 12 hrs, the micromotors were formed.

Characterizations

SEM study was carried out on a FEI 2000 scanning electron microscope with energy dispersive x-ray analysis (EDX) attachment. For the micromotor study, unless otherwise mentioned, the micromotors were placed in solution containing 5 % H_2O_2 and subject to observation under a Nikon eclipse 80i microscope. Optical images and videos were captured by using NIS-Elements D Software. The trajectory and velocity measurement was carried out by utilizing PhysVis software. Magnetic control was realized by applying 1.5 Tesla neodymium (NdFeB) rare earth magnet which was placed 5 cm far from the micromotor. Enzymatic disassembly experiments were performed by mixing the micromotors with lipase from Pseudomonas cepacia at 37 ˚C for different period of time. The reaction system is then sampled on cover glass and observed under Leica DM4000M fluorescence microscope. The amount of the released coumarin was determined using Lambda 750 UV-Vis spectrometer (PerkinElmer Inc.).

Results and discussion
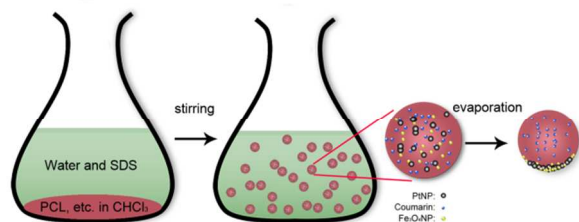
Scheme 1 Schematic illustration indicating the fabrication process.

Scheme 1 illustrates the one-step fabrication route. A typical oil-in-water emulsion[23] was formed under vigorous stirring between a continuous water phase consisting of SDS and a dispersion chloroform phase comprising four components (PCL, PtNP, Fe_3O_4NP and coumarin). Fig. 1A illustrates the optical microscopic image of the emulsion droplet, which has a diameter of approximately 25 μm. During the chloroform evaporation process, since nanoparticles are not miscible with PCL, they phase separated from the rest of the organic phase, accumulated on the droplet surface to reduce interfacial energy between water/oil interface, similar to the Pickering emulsion process.[24,25] After solidification,

nanoparticle agglomerates were pinned at one pole of the colloidal microsphere. The resulting microspheres possess an asymmetric surface compartment containing exposed, catalytically active PtNP and magnetically responsive Fe_3O_4NP, as shown in Fig. 1. Because of the color contrast between PCL polymer and the nanoparticles, it can be clearly seen that the black PtNPs and Fe_3O_4NPs distribute unevenly in the microsphere under an optical microscope (Fig. 1B). Due to the solvent evaporation during the drying process of the emulsion droplet, the size of the dried microstructure is smaller than that of the emulsion droplet. The size distribution of the microsphere is shown in Fig. S1 in ESI†, which has a narrow size distribution with an average size of approximately 18 μm. Fig. 1C is a typical SEM image of the microsphere. The smooth and rough areas are made of PCL polymers/coumarin and nanoparticles, respectively. We have utilized EDX elemental mapping to confirm the surface composition of this microsphere. As indicated in Fig. 1D-E, the smooth area is mainly composed of carbon, oxide, which is the main component of the polymer and coumarin. Other than carbon and oxygen, the rough region exhibits the signals from platinum and iron, indicating the presence of PtNP and Fe_3O_4NP in this area (Fig. 1F-G). Therefore, it can be concluded from the above results that the microsphere consists of polymers with exposed PtNPs and Fe_3O_4NPs segregating onto its surface. Such asymmetric structure is desired for micromotor fabrication to realize autonomous movement of the latter. As compared to the previously developed approaches to attain a micromotor, our one-step method is simple and suitable for mass production.
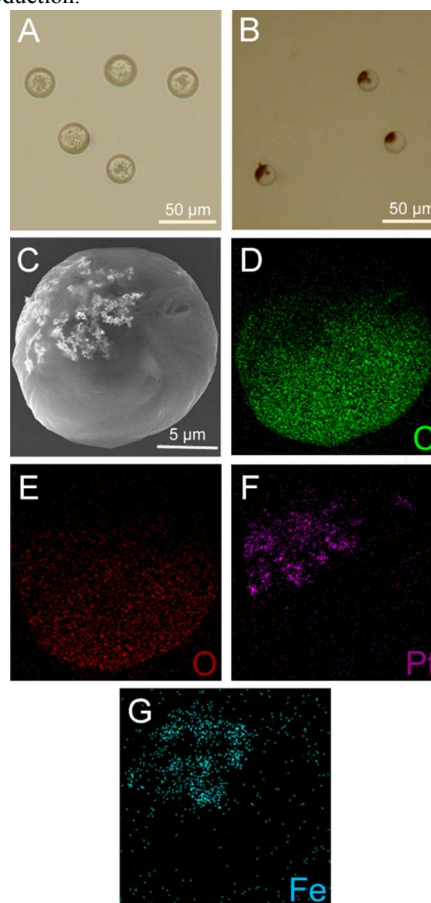
Fig. 1 (A) Optical image of the emulsion droplets. (B) Optical image shows the dried micromotor fabricated by one step method, where the dark and transparent areas can be assigned to PtNPs/Fe$_3$O$_4$NPs and PCL polymer/coumarin, respectively. (C) A typical SEM image of one micromotor. The rough and smooth areas are made of PtNP/Fe$_3$O$_4$NP and PCL polymer/coumarin, respectively. EDX mapping of (D) C, (E) O, (F) Pt and (G) Fe corresponding to the structure shown in (C).

The size of the microsphere can be controlled by adjusting the condition during the fabrication, such as the polymer solution concentration. Fig. S2 in ESI† shows the typical optical microscopic image of the microstructure fabricated at lower PCL concentration, i.e. 30 mg/ml. The resulting microstructures are uniform in size and have an average diameter of approximately 8 μm. By further decreasing the PCL concentration to about 3 mg/ml, a minimum size of about 2 μm can be obtained, as illustrated in Fig. S3A in ESI†. Despite the small size, the corresponding EDX analysis shown in Fig. S3B-D in ESI† confirms the Janus feature.

For a catalytic micromotor, autonomous movement generally relies on the continuous generation of gas bubbles such as oxygen from the surface of the catalytically active areas. The water flux caused by the gas bubble departure leads to the propulsion of the micromotor. Herein, due to the catalytic decomposition of H$_2$O$_2$ on the PtNP side, the as-prepared micromotor moves autonomously once placed in H$_2$O$_2$ aqueous solution based on the above-mentioned bubble propulsion mechanism. Fig. 2 displays four time-lapse images of an individual 18 μm sized micromotor moving autonomously in circles in H$_2$O$_2$ aqueous solution. The images were captured at 2 s interval and the corresponding movie is shown in ESI† as Video S1. A long bubble tail was generated from the PtNP part of the micromotor, propelling the whole structure.
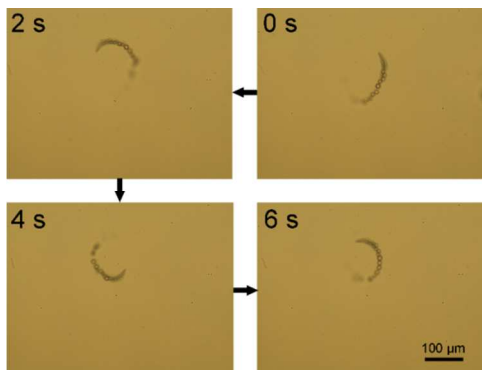
Fig. 2 Four consecutive images taken at 2 s interval from Video S1 in ESI† showing the autonomous movement of the micromotor.

The trajectory of this micromotor is shown in Fig. 3A, based on which the velocity is calculated to be as high as 70 μm/s. On the basis of the weight ratio between PtNP and the rest of the motor (4 mg PtNP vs. 4 mg Fe$_3$O$_4$NP, 20 mg coumarin and 100 mg PCL, i.e. 1:31), PtNPs are capable of carrying about 31 times of its own body weight at a high speed (70 μm/s). Furthermore, we investigated the dependence of the velocity of the catalytic micromotor on the concentration of the fuel molecules in the solution. As shown in Fig.

3B, the average speed decreases from 67 μm/s in the case of 5 % H$_2$O$_2$ to about 38 and 20 μm/s in the case of 3 % and 1 % H$_2$O$_2$, respectively, demonstrating that the speed of the micromotor can be controlled by changing the concentration of H$_2$O$_2$. We further compared the velocity of current micromotor with the previously reported values obtained from other nanoparticle based micromotors. For example, He et al. have reported that the velocity of PtNP-based nanorocket is around 8 μm/s in the presence of 5 % H$_2$O$_2$.[26] Li et al. have shown that their nanoparticle-based polymer micromotor moves at a speed of 10 μm/s in 5 % H$_2$O$_2$.[27] As compared to these literature data, current micromotor moves at a much faster speed, demonstrating the superiority of the current design. The previously utilized PtNPs are protected by surface ligands, such as poly(diallyldimethylammonium chloride) (PDDA)[26] or polyvinylpyrrolidone (PVP),[27] which are known to decrease their catalytic activity.[28] The PtNPs in current study are unprotected, which have higher catalytic activity as compared to the protected ones, leading to higher hydrogen peroxide decomposition rate. As a result, the current micromotor moves faster.
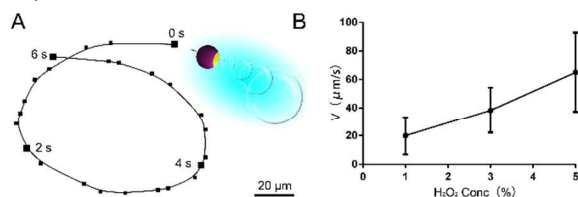
Fig. 3 (A) The trajectory of the micromotor shown in Fig. 2. (B) Fuel concentration dependent velocity of the micromotor.

For micromotors, the capability of moving in complex environment, such as high ionic strength solution is vital for many applications. Although the early reported micromotor based on self-electrophoresis mechanism cannot move in concentrated salt solution,[29] this issue was later solved by the development of tubular microengines.[6] For example, Wang et al. have reported the salt-independent catalytic tubular microengines synthesized by template-assisted method.[20] However, few studies have addressed the salt effect on the nanoparticle-based micromotor. In current case, the micromotor powered by nanoparticles can swim at a high speed in PBS solution containing H$_2$O$_2$, as shown in Video S2 in ESI†. The velocity of the micromotor is estimated to be approximately 62 μm/s in PBS solution, which is slightly lower than that in the H$_2$O$_2$ aqueous solution (67 μm/s). The decrease of the speed may be attributed to the viscosity effect,[18] i.e. 1.05 mPa·s for PBS solution at room temperature as opposed to 1.0 mPa·s for water.[30,31]
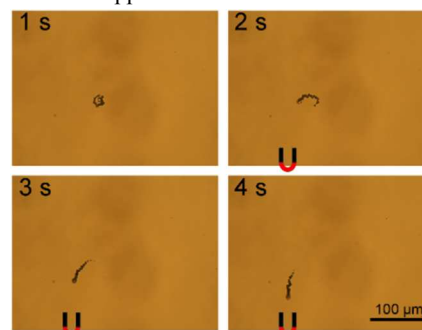
Fig. 4 Time-lapse images taken at 1 s interval from Video S3 in ESI† showing the remote control using the external magnetic field.

In recent years, the ability to manipulate an artificial micromotor by magnetic or other external fields has become increasingly important,[32-34] which is mainly because the movement of a self-propelled micromotor lacks control of the directionality. By introducing the magnetically responsive materials into the micromotor, functions such as targeted navigation[35] and cargo transportation[36] can be achieved which is of great significance for various applications related to micromotors. In general, magnetically responsive materials are deliberately introduced into a micromotor with an extra fabrication step. For example, nickel or iron can be introduced into the micromotors through sequential electrochemical[3] or thermal deposition technique.[6] Recently, efforts have been exerted to the utilization of superparamagnetic nanoparticles as the magnetically responsive materials in micromotors,[27,37] which may avoid the possible aggregation problems caused by the residual magnetism after the magnetic field removal. Additional adsorption step is also exploited in order to immobilize the superparamagnetic nanoparticles onto the micromotor surface. In contrast, the incorporation of magnetically responsive materials in current case can be achieved within one-step by directly adding Fe_3O_4NP to the oil phase during the emulsion droplet formation process. As indicated in Fig. 4, by applying an external magnetic field, the change of the moving direction of an autonomous micromotor in H_2O_2 solution can be realized. The corresponding movie is shown as Video S3 in ESI†. In addition, in contrast to the previously developed magnetic materials used in micromotor, current Fe_3O_4NP is superparamagnetic, making it potentially applicable for direct visualization by magnetic resonance imaging (MRI).[38,39]
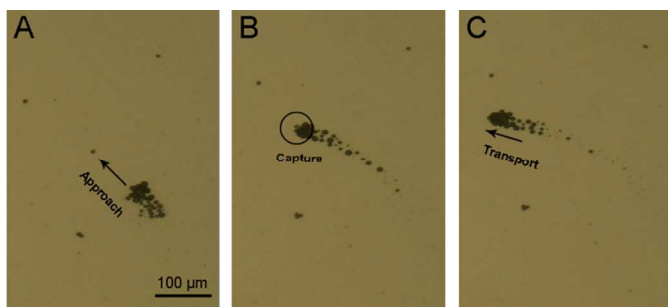
Fig. 5 Time lapse images taken from Video S4 in ESI† indicating one micromotor approaches (A), captures (B) and transports (C) the polystyrene microbead in water containing H_2O_2.

Cargo transportation is one of the most important applications enabled by the micromotors.[40] Based on a variety of different interactions including magnetic interactions, molecular recognition and hydrophobic interactions, various cargoes can be loaded onto the micromotor for transportation, separation or delivery purposes. For example, Wang et al. have reported magnetic micromotors can be used to realize the targeted delivery of drug loaded microparticles toward HeLa cancer cells.[12] Through molecular recognition, the micromotor can be utilized to separate cancer cells,[7] Escherichia coli,[41] etc. from complex environment. Recently, the utilization of

hydrophobic micromotors to gather oil droplet contaminant in water for environmental remediation purpose has also been reported.[42] Since current micromotor can be manipulated by an external magnetic field, we have tested its ability to transport a cargo. Magnetic polystyrene beads were utilized as the model cargoes because they can be captured in the proximity of the micromotor through magnetic interactions, as demonstrated in the literature.[43] As can be seen from Fig. 5A and Video S4 in ESI†, the micromotor can be geared toward the targeted polystyrene bead indicated by the arrow under the guidance of an external magnetic field. In the proximity of the micromotor, the polystyrene bead snaps on due to the magnetic interaction (Fig. 5B), after which the micromotor continuously moves and carries it away (Fig. 5C). Since the polymer body used in this study can be easily functionalized with a variety of different functional groups,[27] current micromotor is potentially applicable to load, transport or separate other cargoes such as proteins and enzymes for sensing or delivery purposes.
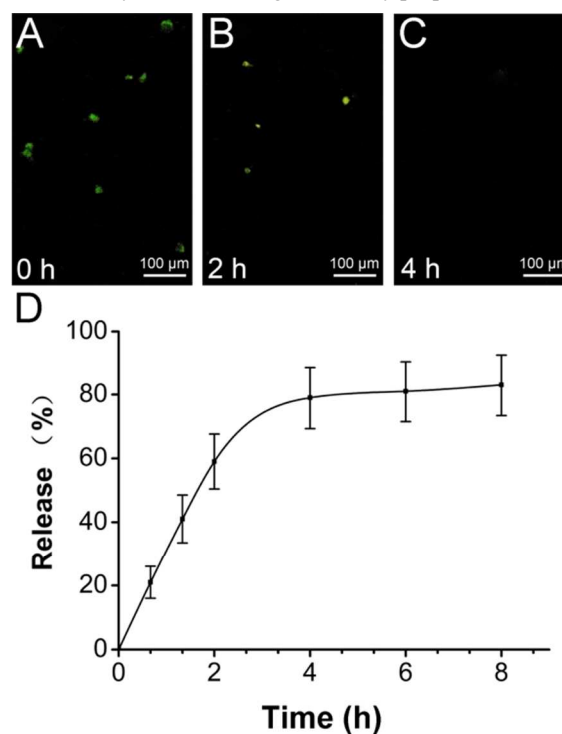
Fig. 6 Fluorescence images showing the coumarin loaded micromotor at different stage of enzymatic treatment (A) 0 hr, (B) 2 hrs and (C) 4 hrs. The enzyme concentration is 2 mg/mL. (D) Sustained release of the coumarin encapsulated inside the micromotor in the presence of 2 mg/mL enzyme.

The controlled release enabled by a micromotor has previously been demonstrated.[26,34,44,45] The release triggered by exposing the micromotor to external stimuli is typically completed within a short period of time. However, for long term therapeutic applications, it is desirable to realize sustained release over a long period of time. The polymeric material utilized in micromotor fabrication (PCL) is an aliphatic polyester, which can slowly degrade in the presence of an enzyme,[46] i.e. lipase from Pseudomonas cepacia. Accompanied by such process, the encapsulated material within PCL can be continuously released. Therefore, by utilizing the biodegradability

Nanoscale Accepted Manuscript

and encapsulation property of PCL, we are able to achieve sustained release for current structure. As a proof-of-concept, we introduced coumarin into the micromotor,[47] which acts as both a model drug and a fluorescent label. Coumarin exhibits green fluorescence under UV irradiation. A series of fluorescence images are shown in Fig. 6A-C, which clearly indicates the disassembly process of the micromotor. At 37 ˚C, in the presence of 2 mg/mL lipase from Pseudomonas cepacia, the micromotor is partially disassembled after 2 hrs **(**Fig. 6B). After 4 hrs, almost all micromotors disassemble (Fig. 6C). Accompanied by this process, the coumarin encapsulated within the micromotor is gradually released and the concentration of coumarin in solution increases accordingly, as shown in Fig. 6D. Most of coumarin is released within the initial 2 hrs, and the rest is sustainably released in the following 2 hrs as the micromotor's disassembly process continues.

As illustrated above, it is easy to incorporate multiple functions such as autonomous movement, magnetic control and encapsulation of various biomaterials into current micromotor, which may lead to drug release application. Furthermore, as compared to the nano/micromagnetic beads (core/shell with various encapsulated materials),[48] the real advantage of these micromotors is that they can move autonomously in solution. The continuous motion of micromotor in solution induces the occurrence of the mixing process, which improves the homogeneity of the solution, leading to the enhancement in the kinetics of the binding reactions. As a result, higher cellular uptake or improved biosensing efficiency, etc. can be achieved by the moving micromotor. For example, He et al. have reported that the amount of the moving micromotor entering the cell is much more than that of the static ones.[49] Merkoci et al. have shown that the moving micromotor exhibits improved biosensing performance (up to 3.5 fold increase as compared to the static ones).[50] Therefore, the autonomous moving property of a micromotor will facilitate its potential application in biomedical field.

Conclusions

In summary, we have demonstrated a facile one-step method to fabricate artificial micromotors utilizing an emulsion solvent evaporation technique. As compared to the previously reported approaches, the current solution-based method is advantageous because the preparation process is simple, low cost, and easy to scale up. More importantly, the fabrication is not simplified at the cost of sacrificing the functions of the micromotor. On the contrary, it is easy to incorporate multiple functions such as autonomous movement, magnetic control, functional material encapsulation, enzymatic disassembly and sustained release into a micromotor within one single step. To the best of our knowledge, it is the first example of the preparation of multifunctional man-made micromotor in such a simplified way, which holds great promise for the practical production in large scale and applications in a variety of different fields.

Acknowledgements

Notes and references

[a]Institute of Functional Nano & Soft Materials (FUNSOM), Jiangsu Key Laboratory for Carbon-Based Functional Materials & Devices and Collaborative Innovation Center (CIC) of Suzhou Nano Science and Technology, Soochow University, Suzhou, Jiangsu 215123, P. R. China, E-mail: bdong@suda.edu.cn
[b]Department of Materials Science and Engineering, Drexel University, Philadelphia 19104, USA, E-mail: chrisli@drexel.edu
[†]Electronic Supplementary Information (ESI) available: Video S1-S4 and Fig. S1-S3. See DOI: 10.1039/b000000x/

1　R. F. Ismagilov, A. Schwartz, N. Bowden and G. M. Whitesides, *Angew. Chem.*, *Int. Ed.*, 2002, **41**, 652-654.
2　W. F. Paxton, K. C. Kistler, C. C. Olmeda, A. Sen, S. K. St Angelo, Y. Y. Cao, T. E. Mallouk, P. E. Lammert and V. H. Crespi, *J. Am. Chem. Soc.*, 2004, **126**, 13424-13431.
3　T. R. Kline, W. F. Paxton, T. E. Mallouk and A. Sen, *Angew. Chem.*, *Int. Ed.*, 2005, **44**, 744-746.
4　S. Sundararajan, P. E. Lammert, A. W. Zudans, V. H. Crespi and A. Sen, *Nano Lett.* 2008, **8**, 1271-1276.
5　J. Wang, *ACS Nano,* 2009, **3**, 4-9.
6　A. A. Solovev, Y. F. Mei, E. B. Urena, G. S. Huang and O. G. Schmidt, *Small*, 2009, **5**, 1688-1692.
7　S. Balasubramanian, D. Kagan, C. M. J. Hu, S. Campuzano, M. J. Lobo-Castanon, N. Lim, D. Y. Kang, M. Zimmerman, L. F. Zhang and J. Wang, *Angew. Chem.*, *Int. Ed.*, 2011, **50**, 4161-4164.
8　M. Guix, C. C. Mayorga-Martinez and A. Merkoci, *Chem. Rev.*, 2014, **114**, 6285-1283.
9　W. Gao and J. Wang, *ACS Nano*, 2014, **8**, 3170-3180.
10　S. Sengupta, M. E. Ibele and A. Sen, *Angew. Chem.*, *Int. Ed.,* 2012, **51**, 8434-8445.
11　D. Patra, S. Sengupta, W. T. Duan, H. Zhang, R. Pavlick and A. Sen, *Nanoscale*, 2013, **5**, 1273-1283.
12　W. Gao, D. Kagan, O. S. Pak, C. Clawson, S. Campuzano, E. Chuluun-Erdene, E. Shipton, E. E. Fullerton, L. Zhang, E. Lauga and J. Wang, *Small*, 2012, **8**, 460-467.
13　W. Gao, X. Feng, A. Pei, Y. Gu, J. Li and J. Wang, *Nanoscale*, 2013, **5**, 4696-4700.
14　W. Gao, A. Pei, X. M. Feng, C. Hennessy and J. Wang, *J. Am. Chem. Soc.*, 2013, **135**, 998-1001.
15　W. Gao, A. Pei, R. Dong and J. Wang, *J. Am. Chem. Soc.*, 2014, **136**, 2276-2279.
16　L. Baraban, D. Makarov, R. Streubel, I. Monch, D. Grimm, S. Sanchez and O. G. Schmidt, *ACS Nano*, 2012, **6**, 3383-3389.
17　F. Z. Mou, C. R. Chen, H. R. Ma, Y. X. Yin, Q. Z. Wu and J. G. Guan, *Angew. Chem.*, *Int. Ed.*, 2013, **52**, 7208-7212.
18　W. Gao, S. Sattayasamitsathit, J. Orozco and J. Wang, *J. Am. Chem. Soc.*, 2011, **133**, 11862-11864.
19　R. Liu and A. Sen, *J. Am. Chem. Soc.*, 2011, **133**, 20064-20067.
20　K. M. Manesh, M. Cardona, R. Yuan, M. Clark, D. Kagan, S. Balasubramanian and J. Wang, *ACS Nano*, 2010, **4**, 1799-1804.
21　G. J. Zhao, A. Ambrosi and M. Pumera, *J. Mater. Chem. A*, 2014, **2**, 1219-1223.
22　C. Hedfors, E. Ostmark, E. Malmstrom, K. Hult and M. Martinelle, *Macromolecules*, 2005, **38**, 647-649.
23　T. G. Mason, J. N. Wilking, K. Meleson, C. B. Chang and S. M. Graves, *J. Phys.: Condens. Mat.*, 2006, **18**, R635-R666.
24　S. U. Pickering, *J. Chem. Soc.*, 1907, **91**, 2001-2021.

25 Z. Niu, J. He, T. P. Russell and Q. Wang, *Angew. Chem., Int. Ed.*, 2010, **49**, 10052-10066.

26 Z. G. Wu, Y. J. Wu, W. P. He, X. K. Lin, J. M. Sun and Q. He, *Angew. Chem., Int. Ed.*, 2013, **52**, 7000-7003.

27 B. Dong, T. Zhou, H. Zhang and C. Y. Li, *ACS Nano*, 2013, **7**, 5192-5198.

28 L. L. Shi, M. Liu, L. M. Liu, W. L. Gao, M. D. Su, Y. Ge, H. Zhang and B. Dong, *Langmuir*, 2014, **30**, 13456-13461.

29 W. F. Paxton, P. T. Baker, T. R. Kline, Y. Wang, T. E. Mallouk and A. Sen, *J. Am. Chem. Soc.*, 2006, **128**, 14881-14888.

30 O. G. Fritz, *Biophys. J.*, 1984, **46**, 219-228.

31 K. Fushimi, and A. S. Verkman, *J. Cell Biol.*, 1991, **112**, 719-725

32 W. Wang, L. A. Castro, M. Hoyos and T. E. Mallouk, *ACS Nano*, 2012, **6**, 6122-6132.

33 S. Ahmed, W. Wang, L. O. Mair, R. D. Fraleigh, S. Li, L. A. Castro, M. Hoyos, T. J. Huang and T. E. Mallouk, *Langmuir*, 2013, **29**, 16113-16118.

34 D. Kagan, M. J. Benchimol, J. C. Claussen, E. Chuluun-Erdene, S. Esener and J. Wang, *Angew. Chem., Int. Ed.*, 2012, **51**, 7519-7522.

35 A. Ghosh and P. Fischer, *Nano Lett.*, 2009, **9**, 2243-2245.

36 S. Tottori, L. Zhang, F. M. Qiu, K. K. Krawczyk, A. Franco-Obregon and B. J. Nelson, *Adv. Mater.*, 2012, **24**, 811-816.

37 M. Liu, L. M. Liu, W. L. Gao, M. D. Su, Y. Ge, L. L. Shi, H. Zhang, B. Dong and C. Y. Li, *Nanoscale*, 2014, **6**, 8601-8605.

38 S. H. Hu and X. H. Gao, *J. Am. Chem. Soc.*, 2010, **132**, 7234-7237.

39 S. Martel, M. Mohammadi, O. Felfoul, Z. Lu and P. Pouponneau, *Int. J. Robot. Res.*, 2009, **28**, 571-582.

40 A. A. Solovev, S. Sanchez, M. Pumera, Y. F. Mei and O. G. Schmidt, *Adv. Funct. Mater.*, 2010, **20**, 2430-2435.

41 S. Campuzano, J. Orozco, D. Kagan, M. Guix, W. Gao, S. Sattayasamitsathit, J. C. Claussen, A. Merkoci and J. Wang, *Nano Lett.*, 2012, **12**, 396-401.

42 M. Guix, J. Orozco, M. Garcia, W. Gao, S. Sattayasamitsathit, A. Merkoci, A. Escarpa and J. Wang, *ACS Nano*, 2012, **6**, 4445-4451.

43 J. Burdick, P. Laocharoensuk, P. M. Wheat, J. D. Posner and J. Wang, *J. Am. Chem. Soc.*, 2008, **130**, 8164-8165.

44 F. Z. Mou, C. R. Chen, Q. Zhong, Y. X. Yin, H. R. Ma and J. G. Guan, *ACS Appl. Mater. Interfaces*, 2014, **6**, 9897-9903.

45 Y. J. Wu, Z. G. Wu, X. K. Lin, Q. He and J. B. Li, *ACS Nano*, 2012, **6**, 10910-10916.

46 Z. H. Gan, Q. Z. Liang, J. Zhang and X. B. Jing, *Polym. Degrad. Stab.*, 1997, **56**, 209-213.

47 N. Farinola and N. Piller, *Lymphat. Res. Biol.*, 2005, **3**, 81-86.

48 W. Wu, Z. H. Wu, T. K. Yu, C. Z. Jiang and W. S. Kim, *Sci. Technol. Adv. Mater.* 2015, **16**, 023501.

49 M. J. Xuan, J. X. Shao, X. K. Lin, L. R. Dai and Q. He, *ChemPhysChem*, 2014, **15**, 2255-2260.

50 E. Morales-Narvaez, M. Guix, M. Medina-Sanchez, C. C. Mayorga-Martinez and A. Merkoci, *Small*, 2014, **10**, 2542-2548.